



FILTER-BASED FIRST- AND HIGHER-ORDER DIFFRACTION MODELING

Christoph Kirsch*

Stephan D. Ewert

Medizinische Physik and Cluster of Excellence Hearing4All,
Carl von Ossietzky Universität Oldenburg, Germany

ABSTRACT

Applications for complex acoustic environments exist in, e.g., hearing research, architectural planning, and entertainment. Geometrical acoustics (GA) offers a high computational efficiency, as required for dynamic real-time renderings. However, the assumed ray-like propagation does not directly account for perceptually relevant effects of diffraction, which are particularly noticeable for occluded sound sources. In typical indoor environments, finite objects and apertures like, e.g., tables, billboards, and doors form an important category of entities, for which computationally efficient diffraction modelling is of interest.

Here, we apply a recent approach for integrating diffraction into GA to a flat finite object. The underlying universal diffraction filter approximation (UDFA) uses (fractional-order) filter functions with physically-based parameters to account for first-order edge diffraction. Higher-order diffraction, i.e., repeated diffraction at the same object leads to additional spectral effects at low frequencies which are modelled in a simplified way using additional filters. The suggested filter approach and topology offer a computationally highly efficient and spatially smooth infinite impulse response (IIR) implementation for modelling diffraction. Results are compared to a state-of-art higher-order diffraction simulation technique.

Keywords: *digital filters, scattering, virtual acoustics, geometrical acoustics*

*Corresponding author: christoph.kirsch@uol.de.

Copyright: ©2023 Christoph Kirsch and Stephan D. Ewert. This is an open-access article distributed under the terms of the Creative Commons Attribution 3.0 Unported License, which permits unrestricted use, distribution, and reproduction in any medium, provided the original author and source are credited.

1. INTRODUCTION

Virtual acoustic environments (VAEs) are created using propagation models to evoke a listening experience resembling a particular real or imaginary indoor or outdoor environment. Due to their high computational efficiency, geometrical acoustics (GA) is frequently used to model direct sound and early reflections, assuming ray-like propagation and specular reflections. To account for perceptually relevant effect of diffraction and to provide an overall continuous sound field at geometric boundaries, where, e.g., the direct sound path becomes occluded, additional paths with modified spectral content are required [1-3].

Keller [4] proposed a description of diffraction in the framework of geometrical optics with an asymptotic solution for infinite wedges, offering an easier-to-manage expression compared to previous (exact) solutions (e.g., Biot-Tolstoy [5]). Subsequently, other asymptotic solutions were proposed, applicable to a wider range of geometrical configurations, and using varying numbers of diffraction terms: Pierce [6] used two or three terms, and Kouyoumjian and Pathak [7] used four terms.

In many applications diffraction from finite wedges is relevant. Medwin [8] adapted the previous Biot-Tolstoy solution [5] to finite wedges. Svensson et al. [9] reformulated the expression proposed by Medwin [8], forming a line integral over so-called secondary sources along the wedge. This solution (referred to as Biot-Tolstoy-Medwin-Svensson, BTMS, in the following) is convenient and is also available in the frequency domain [10]. Being based on secondary sources along the wedge, BTMS can also be used for the computation of higher-order (HO) diffraction [11], e.g., from repeated diffraction at different edges of an object. HO diffraction leads to spectral effects predominantly at low frequencies (e.g., [9, 12, 13]). For finite reflectors, a high-

pass effect is observed (see also [14, 15]). All above diffraction solutions are computationally quite involved and are not directly applicable for real-time VAEs, particularly considering HO diffraction.

Recently, filter-based diffraction solutions were proposed [16, 17, 18], offering a physically-based, computationally highly-efficient method to model diffraction from arbitrary infinite and finite wedges. Ewert [17] derived filter representations of the asymptotic solutions [6, 7] and an approximation of BTMS in both frequency and time domain, based on modified fractional-order transfer functions and the corresponding impulse response. Diffracted sound is parametrized by cutoff frequencies derived from the geometry at the edge. The universal diffraction filter approximation (UDFA; [18]) introduces simplifications for finite edges and proposes a recursive filter design. Furthermore, it was demonstrated that diffraction by flat, rectangular plate can be characterized by superimposing the four individually filtered edge paths.

For virtual acoustics applications, a continuous “smooth” sound field is important for perceptual plausibility (see also e.g., Pulkki and Svensson [19]), when sound sources and/or receivers are moving in the virtual space. Likewise, the “shadow” of small finite objects must disappear at larger distances. With the visibility-dependence of the GA direct sound and specular reflection paths, an accurate continuous sound field in VAEs can only be achieved by integrating diffraction effects.

In this contribution, we apply UDFA to two example cases highly relevant for interactive acoustics simulations: the square edge (e.g., a building or room corner) and a flat plate (e.g., a table or screen). It is demonstrated, how a continuous sound field is achieved for arbitrary geometrical arrangements of source, receiver and object using first-order diffraction for effects of HO diffraction. For both example cases, we propose a highly-efficient infinite impulse response (IIR) filter architecture enabling smooth transitions of the approximated sound field across the GA shadow and reflection boundaries and a heuristic approximation of the spectral effects of HO diffraction at low frequencies. The results are compared to the BTMS reference solution. This paper is structured as follows: Section 2 outlines the wedge diffraction problem and UDFA. In Section 3, architectures are proposed for spatially smooth sound rendering at room corners and flat finite objects. Section 4 discusses and summarizes the results.

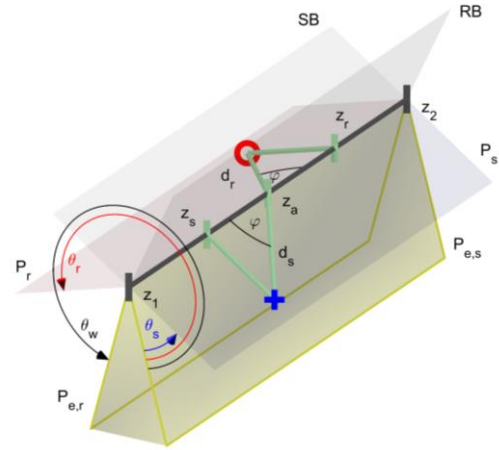


Figure 1. Two intersecting planes, $P_{e,s}$ and $P_{e,r}$, form a wedge located on the longitudinal z -axis of a cylindrical coordinate system, extending from z_1 to z_2 , ($\pm\infty$ for an infinite wedge). Source (blue cross) and receiver (red circle) are located in the planes P_s and P_r (grey) at angles θ_s and θ_r , with all azimuth angles referenced to $P_{e,s}$. The shortest path between source and receiver intersects the edge at an angle φ at apex point z_a . The exterior wedge angle is referred to as θ_w . SB and RB denote the shadow and reflection boundary, respectively.

2. FILTER-BASED DIFFRACTION MODELING

A rigid infinite or finite wedge along the z -axis of a cylindrical coordinate system is considered, formed by two intersecting planes as shown in Fig. 1. The source (blue cross) is arbitrarily assumed to be closer to either wedge plane $P_{e,s}$ than the receiver (red circle), reflecting reciprocity of the problem. All azimuth angles θ are referenced to $P_{e,s}$. The receiver wedge plane $P_{e,r}$, is located at the exterior wedge angle θ_w . Source and receiver are located in the planes P_s and P_r with axial coordinates z_s , z_r , radial distances r_s , r_r , and azimuth angles θ_s , θ_r , respectively. At the apex point z_a , the incidence angle φ between edge and vector to the source in plane P_s equals the angle between edge and vector to the receiver in plane P_r . Past the shadow boundary (SB) at $\theta_s + \pi$, the source becomes invisible to the receiver and only the diffracted

field exists (referred to as shadow zone, SZ). In addition to the incident GA sound field in the “view” or “illuminated” zone (VZ), there is a reflected GA sound field in the reflection zone (RZ), separated by the reflection boundary (RB) at $\pi - \theta_s$ from the VZ. A diffracted transmission path between the source and receiver can be constructed using the apex point z_a on the the edge, which serves as a center node. The distances between source and receiver and the apex point z_a are d_s and d_r , respectively.

Based on Ewert [17], UDFA [18] describes the diffracted sound by the superposition of a scalable number of one to four modified fractional-order low-pass filters. For general virtual acoustics applications, using two terms is recommended, where the (infinite edge) cutoff frequencies for the low-pass filters are derived from the geometry at the wedge as

$$f_{c\pm}(\theta) = \frac{2c}{\pi^2 d^* \sin^2(\varphi)} [N_{v\pm}(\theta)]^2. \quad (1)$$

Here $d^* = 2d_s d_r / d$ is the characteristic distance and

$$N_{v\pm}(\theta) = \frac{v \sqrt{1 - \cos(v\pi)} \cos(v\theta)}{\cos(v\pi) - \cos(v\theta)}, \quad (2)$$

expresses the dependency of $f_{c\pm}$ on the source and receiver positions and the exterior wedge index v .

Filter gains are calculated as

$$g_{v\pm}(\theta) = \frac{\sin(v\pi)}{(1 - \cos(v\pi) \cos(v\theta))^{1/2}}. \quad (3)$$

Eqn. 1-3 are evaluated for $\theta_- = \theta_s - \theta_r$ and $\theta_+ = \theta_s + \theta_r$, resulting in two diffraction filters with the transfer function

$$H(f) = ((jf/f_c)^{2/b} + (jf/Qf_c)^{1/b^r} + 1)^{-\alpha b/2}.$$

Here, $\alpha = 0.5$ is the fractional filter order and the parameters $b = 1.44$, $Q = 0.2$, and $r = 1.6$, provide a smooth roll-off around the cutoff frequency.

For a detailed theoretical description, see [17] and for the finite wedge approximation method and IIR implementation, see [18].

3. ZONE TRANSITIONS

3.1 Room corner

Fig. 2 shows the transition between SZ and VZ at an infinite wedge with an exterior wedge angle $\theta_w = 270^\circ$, approximating of a typical room corner with rigid floor and ceiling. The right panel of Fig. 2 shows a projection of the radial plane (view in z-direction), with the receiver position indicated by a red circle and different sound source positions

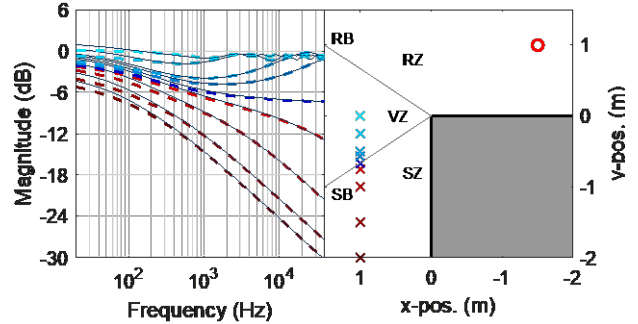


Figure 2. Left panel: Magnitude transfer functions of the sound field at an infinite square wedge for different sound source positions. Colored, dashed traces: UDFA; thin, black, solid traces: BTMS. The right panel shows the wedge (shaded, view in z-direction), and the receiver (red circle) and sound source locations (crosses, color coded matching the left panel). The shadow- and reflection boundary (SB, RB) are indicated by thin grey lines, separating shadow zone (SZ), view zone (VZ) and reflection zone (RZ).

indicated by colored crosses. The left panel shows the corresponding color-coded magnitude transfer functions. In the SZ (red traces), where only diffracted sound arrives at the receiver, the traces show a low-pass characteristic. The cutoff frequency rises with decreasing distance to the SB. The slope of the filter is -3 dB/Oct. At the SB, (dark blue) a high shelving characteristic is observed with a gain of -6 dB. In the VZ, the sum of diffracted and direct sound oscillates around the flat frequency response corresponding to the direct sound alone. With increasing distance to the SB, the ripples diminish.

For an efficient real-time implementation with recursive filters, we propose the design illustrated in Fig. 3. Direct sound and reflected sound are switched on and off, based on visibility checks, with GA propagation attenuation and delay. Diffracted sound is implemented using the serial shelving filter design described in [18], and a separate phase-inversion stage at the output of each filter stage. Here, two parallel diffraction filters with the transfer functions $H_{diff,1}$ and $H_{diff,2}$ are used (two-term solution from [18]). For increased accuracy, up to four of these filters can be used. The diffraction path length determines attenuation and delay.

Key to a “smooth” rendering is that the diffraction path is always present. At the SB and RB, the length of the diffracted path matches that of the direct or reflected sound path, respectively.

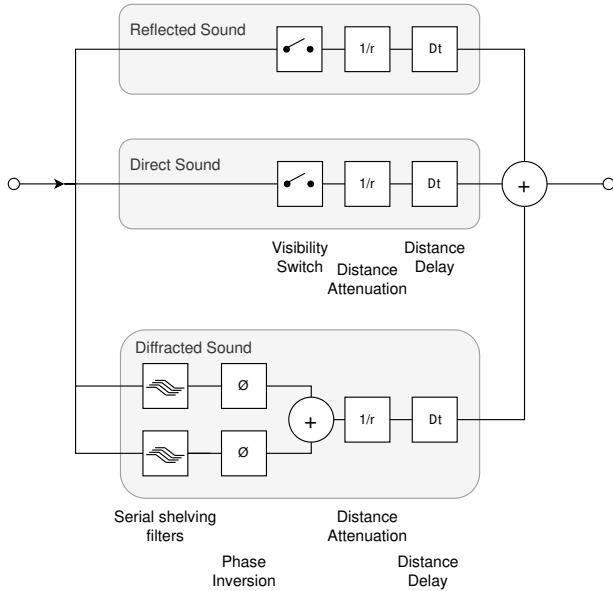


Figure 3. Block diagram for filter-based, spatially smooth diffraction auralization. In addition to direct and geometrically reflected sound, two diffraction filters are rendered, for which the output can be individually phase-inverted while retaining their IIR filter states.

For further illustration, the SB transition is shown in Fig. 4. The solid blue line is a replot from Fig. 2 and shows the overall magnitude response at the SB. The grey, horizontal line indicates the GA direct sound component, which asymptotes the overall sound at low frequencies. The dotted green traces indicate the outputs of the two diffraction filters. The diffracted reflected sound shows a low-pass characteristic, whereas the diffracted incident sound shows a flat frequency response, given that the cutoff frequency for this component rises to infinity at the SB (and the diffraction impulse response becomes a delta pulse, see also [17, 20, 21]). For this diffraction component, a polarity switch occurs at the SB. The dashed brown line illustrates the sum of both diffraction components when they are out of phase. A smooth transition with this phase switch is achieved, given that

$$H_{\text{dir}} - H_{\text{diff},1} + H_{\text{diff},2} = H_{\text{diff},1} + H_{\text{diff},2}, \quad (4)$$

with $H_{\text{diff},1} = H_{\text{dir}}/2$ at the SB where $f_{c,1} = \infty$ and $g_1 = 1/2$, according to Eqn. (1) and (3).

At the RB, the same behavior as in Fig. 4 and Eqn. (4) is observed for the diffracted reflected component with $f_{c,2} = \infty$ and $g_2 = 1/2$.

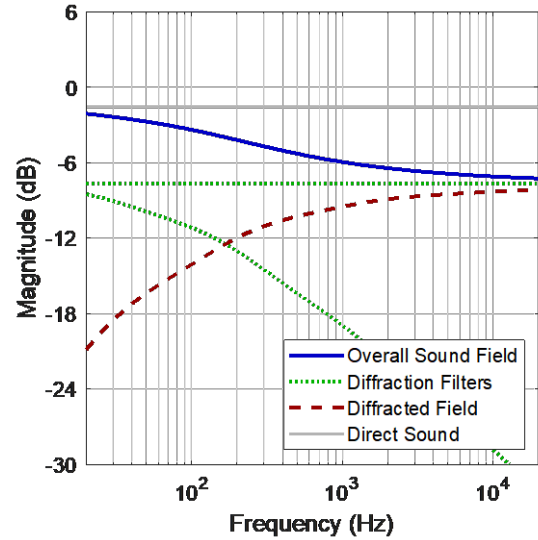


Figure 4. Transfer function of components of the sound field at the SB. The blue, solid trace is a replot from Fig. 2 and shows the overall sound field at the SB. The green, dotted traces correspond to the individual diffraction filters. The brown, dashed trace is the sum of both diffraction components if one phase is inverted.

3.2 Flat plate

We assume that flat objects like tables and billboards can be approximated by an idealized two-dimensional, rigid plate, composed of several finite edges for which diffraction is modelled using UDFA. For a comparison between a measurement of a real plate and UDFA, see [18].

In order to approximate the spectral effects of HO diffraction and to ensure a smooth sound field around the object, we propose the rendering architecture illustrated in Fig. 5. The sound is split by a set of complementary first-order high- and low-pass filters. The low-pass part is always rendered, regardless of visibility. The path length either corresponds to the GA direct sound or, if occluded, to the shortest diffraction path. The high-pass part is rendered as described in Sec. 3.2, with a separate diffraction path for each edge of the object.

As suggested in [18], the cross-over frequency for the complementary filters is based on Rindel [14, 15], who proposed a limiting frequency f_g for rectangular reflectors, above which diffraction losses at a reflector “can be considered negligible”:

$$f_g = \frac{cd^*}{2S \cos(\gamma)}, \quad (5)$$

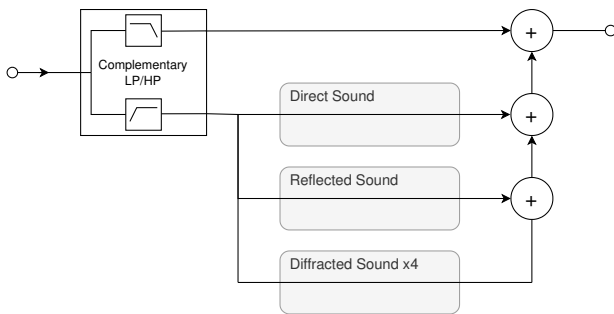


Figure 5. Rendering architecture for spatially smooth sound around a finite flat object.

where d^* is the characteristic distance to the reflection point, S is the surface area of the reflector and γ is the angle between the plate normal and a geometrical reflection on the plate (or extension thereof). Since first-order diffraction is already accounted for by UDFA, $f_g/2$ is used as the cross-over frequency.

We propose a modification to the definition of γ in order to achieve a smooth sound field: The point from which γ is calculated is constrained to be within the plate if the geometrical reflection point is outside the plate and the GA reflection disappears. This results in two different angles γ_s and γ_r for the source and receiver, respectively. The larger angle is used in Eqn. (5), resulting in $f_g \rightarrow \infty$ when source or receiver are located in the object plane.

When the source is visible, the complementary cross-over filters result in a flat response for the direct sound component. Depending on the object size and the geometrical arrangement, the diffracted and reflected sound are high-pass filtered, reducing errors at low frequencies, most notably for objects acting as finite reflectors.

Fig. 6 shows the magnitude transfer functions for different sound source positions indicated by crosses in the top panel. In the left column, first-order diffraction is considered for both the BTMS reference (thin, solid) and UDFA (dashed). In the right column HO-BTMS (15th order) and UDFA with proposed architecture is shown.

Panel a) and b) shows the overall sound field for source positions 1-3 on the plate side opposite to the receiver (red circle). At position 1, the sound source is centered behind the plate, and the four diffraction paths are identical. The reference exhibits spectral ripples, which are not represented by UDFA. First- and HO diffraction differ at low frequencies, where HO diffraction results in a low-shelving characteristic. Position 2 is located at the SB, where a transition occurs that is conceptually similar to the one described in Sec. 3.1. Spectral ripples in the reference at high frequencies are reproduced by UDFA, given that they are

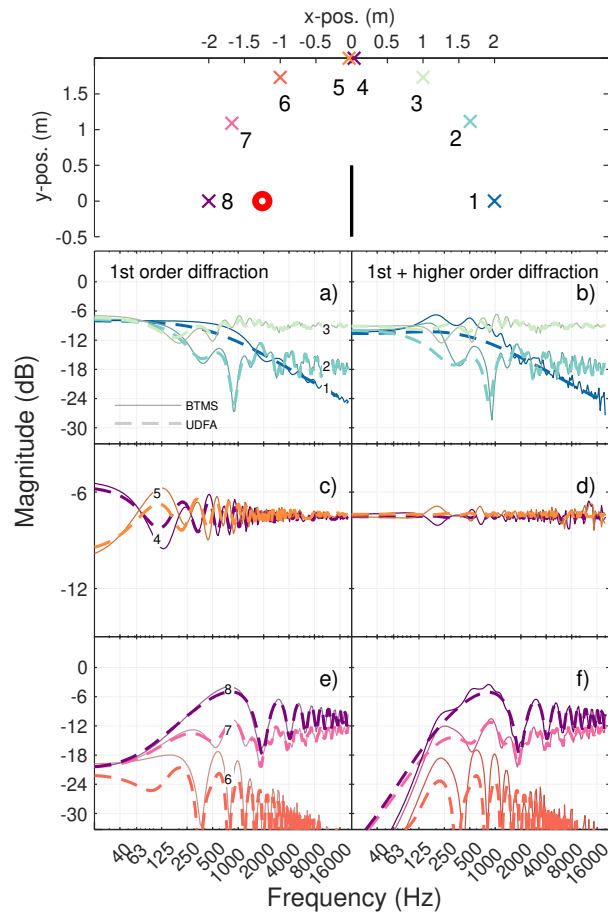


Figure 6. Transfer functions for different source positions near a plate. Top panel: geometrical arrangement of the plate (black line, view from above in the plate plane). Receiver (red circle) and sound source positions indicated by colored crosses. Left column: first-order diffraction, BTMS (thin, solid) and UDFA (dashed). Right column: HO-BTMS (15th order) and UDFA with the architecture according to Fig. 5. Note that the y-axis scale is magnified in panels c) and d) for improved clarity.

mainly caused by path differences of the contributions from the individual edges. In b), the effect of HO diffraction is reproduced by UDFA, matching the reference at very low frequencies. However, the proposed architecture may introduce deviations due to path differences between the diffraction paths and the low-pass component, e.g., for position 2 at around 125 Hz.

Panels c) and d) show the response for sound sources located very close to either side of the plate-plane (position 4 and 5). Because position 5 is located closer to the receiver than position 4, there is a frequency-independent level difference. When only first-order diffraction is considered in panel c), a phase switch of the ripples is observed for BTMS and UDFA, causing a discontinuity for the plate-plane transition. This is caused by a direct transition from SZ to RZ for the edges of the idealized flat object. The HO-BTMS reference in panel d) exhibits considerably smaller ripples compared to first-order diffraction, especially at low frequencies. The HO response is reproduced by UDFA with the proposed crossover filters, for which f_g converges towards infinity as sound source or receiver approach the plate-plane. Consequently, the high-pass part containing spectral ripples caused by the superposition of diffracted and direct sound disappears, and a flat frequency response is rendered below the infinite crossover frequency f_g .

The source positions in panel e) and f) are mirrored versions of those in panel a) and b). For clarity, the direct sound is disregarded in the transfer function plots. For position 6, no geometrical reflection is present, and a -3 dB/Oct envelope low-pass behavior is observed at high frequencies. Position 7 is located at the RB. The corresponding transfer functions are attenuated by about 6 dB in the mid frequencies and converge to those of position 8 at high frequencies. The geometrical reflection point is at the center of the plate for position 8. The transfer functions oscillate around a flat frequency response at high frequencies. As previously described in [12, 13, 18], first-order diffraction (panel e), leads to a low-frequency shelving characteristic, whereas, for HO diffraction, a high-pass characteristic is observed. The high-pass slope for HO-BTMS is steeper (approx. 12 dB/Oct) than that of the proposed UDFA first-order crossover filter.

4. DISCUSSION AND CONCLUSION

It has been shown that augmenting GA with diffraction paths using UDFA results in a spatially smooth sound field at an infinite wedge.

For composed flat objects, additional complementary filters were suggested that ensure a smooth sound field and heuristically approximate the spectral effects of HO diffraction. The suggested architecture covers important classes of entities in virtual acoustic environments (corners, flat plates) and can be incorporated into typical GA-based rendering systems. Reflections, including HO diffraction effects from finite objects would be based on the high-pass part of the suggested crossover filter structure shown in

Fig. 5. The current approach differs from, e.g., a previous machine-learning-based approach [19], offering a physically-based solution for the infinite wedge case and a physically motivated filter architecture for objects.

A potential limitation is that the suggested first-order crossover filters are not steep enough to match HO diffraction, mostly apparent for the high-pass effect for finite reflectors. A (computationally more expensive) second-order high-pass and complementary low-pass filter would be more adequate, however do not straightforwardly result in a smooth frequency response when recombined with different gains.

In the future, the current approach can be adapted to three-dimensional objects and a perceptual evaluation is required.

5. ACKNOWLEDGMENTS

This work was funded by the Deutsche Forschungsgemeinschaft, DFG – Project-ID 352015383 – SFB 1330 C5.

6. REFERENCES

- [1] R. Torres, U. P. Svensson, and M. Kleiner, “Computation of edge diffraction for more accurate room acoustics auralization,” *J. Ac. Soc. Am.*, vol. 109, no. 2, pp. 600–610, Feb. 2001, doi: 10.1121/1.1340647.
- [2] R. Torres, M. Kleiner, and B.-I. Dalenbäck, “Audibility of ‘Diffusion’ in Room Acoustics Auralization: An Initial Investigation,” *Acta Acustica united with Acustica*, vol. 86, pp. 919–927, Nov. 2000.
- [3] T. Lokki, U. P. Svensson, and L. Savioja, “An efficient auralization of edge diffraction,” *Proc. AES 21st International Conference*, St. Petersburg, Russia, Jun. 2002.
- [4] J. B. Keller, “Geometrical Theory of Diffraction,” *J. Opt. Soc. Am.*, vol. 52, no. 2, pp. 116–130, Feb. 1962, doi: 10.1364/JOSA.52.000116.
- [5] M. A. Biot and I. Tolstoy, “Formulation of Wave Propagation in Infinite Media by Normal Coordinates with an Application to Diffraction,” *J. Ac. Soc. Am.*, vol. 29, no. 3, pp. 381–391, Mar. 1957, doi: 10.1121/1.1908899.
- [6] A. D. Pierce, “Diffraction of sound around corners and over wide barriers,” *J. Ac. Soc. Am.*, vol. 55, no. 5, pp. 941–955, May 1974, doi: 10.1121/1.1914668.

- [7] R. G. Kouyoumjian and P. H. Pathak, “A uniform geometrical theory of diffraction for an edge in a perfectly conducting surface,” *Proc. IEEE*, vol. 62, no. 11, pp. 1448–1461, Nov. 1974, doi: 10.1109/PROC.1974.9651.
- [8] H. Medwin, “Shadowing by finite noise barriers,” *J. Ac. Soc. Am.*, vol. 69, no. 4, pp. 1060–1064, Apr. 1981, doi: 10.1121/1.385684.
- [9] U. P. Svensson, R. I. Fred, and J. Vanderkooy, “An analytic secondary source model of edge diffraction impulse responses,” *J. Ac. Soc. Am.*, vol. 106, no. 5, pp. 2331–2344, Oct. 1999, doi: 10.1121/1.428071.
- [10] U. P. Svensson, P. T. Calamia, and S. Nakanishi, “Frequency-Domain Edge Diffraction for Finite and Infinite Edges,” *Acta Acustica united with Acustica*, vol. 95, no. 3, pp. 568–572, May 2009, doi: 10.3813/AAA.918181.
- [11] A. Asheim and U. Peter Svensson, “An integral equation formulation for the diffraction from convex plates and polyhedra,” *J. Ac. Soc. Am.*, vol. 133, no. 6, pp. 3681–3691, Jun. 2013, doi: 10.1121/1.4802654.
- [12] R. R. Torres, N. de Rycker, and M. Kleiner, “Edge Diffraction and Surface Scattering in Concert Halls: Physical and Perceptual Aspects,” *J. Temporal Design Architecture Environment*, vol. 4, no. 1, p. 7, 2004.
- [13] U. P. Svensson, S. R. Martin, J. Šlechta, J. E. Summers, B. H. Teres, and C. F. Gaumont, “Accuracy aspects for diffraction-based computation of scattering,” *Proc. of Euronoise 2018, Crete*.
- [14] J. H. Rindel, “Attenuation of Sound Reflections due to Diffraction,” *Proc. Nordic Acoustical Meeting, Aalborg, Denmark, 1986*.
- [15] J. H. Rindel, “Acoustic Design of Reflectors in Auditoria,” *Proc. of the Institute of Acoustics*, vol. 14, no. 2, pp. 119–129, 1992.
- [16] C. Kirsch and S. D. Ewert, “Low-Order Filter Approximation of Diffraction for Virtual Acoustics,” *IEEE Workshop on Applications of Signal Processing to Audio and Acoustics (WASPAA)*, New Paltz, NY, USA, 2021, pp. 341–345. doi:10.1109/WASPAA52581.2021.9632674.
- [17] S. D. Ewert: “A filter representation of diffraction at infinite and finite wedges,” *JASA Express Lett.* 2, 092401 (2022), doi: 10.1121/10.0013686.
- [18] C. Kirsch, and S. D. Ewert: „A Universal Approximation of Edge Diffraction for Virtual Acoustics,” *IEEE/ACM Trans. Audio, Speech, Language Process.*, 2023, doi: 10.1109/TASLP.2023.3264737, in press.
- [19] V. Pulkki and U. P. Svensson, “Machine-learning-based estimation and rendering of scattering in virtual reality,” *J. Ac. Soc. Am.*, vol. 145, no. 4, pp. 2664–2676, Apr. 2019, doi: 10.1121/1.5095875.
- [20] T. W. Veruttipong, “Time domain version of the uniform GTD,” *IEEE Transactions on Antennas and Propagation*, vol. 38, no. 11, pp. 1757–1764, Nov. 1990, doi: 10.1109/8.102736.
- [21] P. R. Rousseau and P. H. Pathak, “TD-UTD for scattering from a smooth convex surface,” in *IEEE Antennas and Propagation Soc. International Symposium. 1996 Digest*, Jul. 1996, pp. 2084–2087 vol.3. doi: 10.1109/APS.1996.550019.